Multigrid Solution of the Euler Equations Using Implicit Schemes

Antony Jameson* and Seokkwan Yoon†
Princeton University, Princeton, New Jersey

A multigrid method for implicit schemes of the approximate factorization type is described. The application of the method coupled with an alternating direction implicit scheme to the solution of the Euler equations for transonic flow over an airfoil has resulted in very rapid convergence. The number of time steps required to reach a steady state is reduced by an order of magnitude by the introduction of multiple grids.

I. Introduction

MULTIGRID has emerged as a particularly efficient technique for accelerating the convergence of numerical calculations. While the available theorems in the theory of multigrid methods generally assume ellipticity, it seems that it ought to be possible to accelerate the evolution of a hyperbolic system to a steady state by using large time steps on coarse grids, so that disturbances are more rapidly expelled through the outer boundary. It has been established that the multigrid method can dramatically accelerate the convergence of transonic potential flow calculations, although the governing equations are of mixed elliptic and hyperbolic type.[1] For the Euler equations a multigrid scheme proposed by Ni has widely been used.[2] In its published form his distributed correction scheme includes an artificial dissipation term that restricts the results to first-order accuracy. A new multigrid method which is second-order-accurate in space was developed for the multistage explicit time stepping scheme.[3] Since the time step of an explicit scheme is limited by the Courant-Friedrichs-Lewy (CFL) condition, which requires that the region of dependence of the difference scheme must at least include the region of dependence of the differential equation, an implicit scheme is preferred as the driving scheme. Two general types of implicit schemes can be distinguished, those using residual averaging, and those based on approximate factorization. Recently the multigrid method was successfully introduced for the implicit multistage scheme[4] which belongs to the residual averaging type. In this paper it is shown that the schemes of the approximate factorization type can be adapted for use in conjunction with a multigrid technique to produce a rapidly convergent algorithm for calculating steady-state solutions of the Euler equations.

II. Semidiscrete Finite Volume Scheme

The Euler equations in integral form can be written as:

$$\frac{\partial}{\partial t}\iiint_{\Omega} w\,\mathrm{d}\Omega + \iint_{\partial\Omega} \underline{F}\cdot \mathrm{d}\underline{S} = 0 \tag{1}$$

for a fixed region Ω with boundary $\partial\Omega$. Here w represents the conserved quantity and F is the corresponding flux term. If we write p, ρ, u, v, $\bar{E}$ and H for the pressure, density, Cartesian velocity components, total energy and total enthalpy, then Eq. (1) represents mass conservation if we put

$$w=\rho,\quad \underline{F}=(\rho u,\rho v)$$

For conservation of momentum in the x direction we have

$$w=\rho u,\quad \underline{F}=(\rho u^2+p,\rho uv)$$

in Eq. (1). Conservation of momentum in the y direction is similarly defined. Finally energy conservation is given by

$$w=\rho E,\quad \underline{F}=(\rho Hu,\rho Hv)$$

These equations are to be solved for a steady-state $\partial w/\partial t=0$ where t denotes time.

A convenient way to assure a steady-state solution independent of the time step is to separate the space and time discretization procedures. In a semidiscrete finite volume scheme one begins by applying a semidiscretization in which only the spatial derivatives are approximated. In order to derive a semidiscrete model which can be used to treat complex geometric domains, the computational domain is divided into quadrilateral cells. Assuming that the dependent variables are known at the center of each cell, a system of ordinary differential equations is obtained by applying Eq. (1) separately to each cell. These have the form

$$\frac{\mathrm{d}}{\mathrm{d}t}(S_{ij}w_{ij})+Q_{ij}=0 \tag{2}$$

where S_{ij} is the cell area, and Q_{ij} is the net flux out of the cell. This can be evaluated as

$$\sum_{k=1}^{4}(\Delta y_k f_k-\Delta x_k g_k) \tag{3}$$

where f_k and g_k denote values of the flux vectors f and g on the kth edge, Δx_k and Δy_k are the increments of x and y along the edge with appropriate signs, and the sum is over the four sides of the cell. The flux vectors are evaluated by taking the average of the values in the cells on either side of the edge:

$$f_2=\tfrac{1}{2}(f_{i+1,j}+f_{i,j}) \tag{4}$$

for example. The scheme constructed in this manner reduces to a central difference scheme on a Cartesian grid and is second-order-accurate in space provided that the mesh is smooth enough. It also has the property that uniform flow is an exact solution of the difference equations.

Presented as Paper 85-0293 at the AIAA 23rd Aerospace Sciences Meeting, Reno, NV, Jan. 14-17, 1985; received Feb. 28, 1985; revision received Feb. 3, 1986.

*Professor, Department of Mechanical and Aerospace Engineering. Member AIAA.

†Graduate Research Assistant, Department of Mechanical and Aerospace Engineering. Member AIAA.

III. Adaptive Dissipation

In order to suppress the tendency for spurious odd and even point oscillations, and to prevent unsightly overshoots near shock waves, the scheme is augmented by a dissipative term so that Eq. (2) becomes

$$\frac{\mathrm{d}}{\mathrm{d}t}(S_{ij}w_{ij}) + Q_{ij} - D_{ij} = 0 \tag{5}$$

Here D_{ij} is the dissipation, which is constructed so that it is of third order in smooth regions of the flow. For the density equation $D_{ij}(\rho)$ has the form

$$d_{i+\frac{1}{2},j} - d_{i-\frac{1}{2},j} + d_{i,j+\frac{1}{2}} - d_{i,j-\frac{1}{2}} \tag{6}$$

where

$$d_{i+\frac{1}{2},j} = \epsilon^{(2)}_{i+\frac{1}{2},j}(\rho_{i+1,j} - \rho_{i,j}) - \epsilon^{(4)}_{i+\frac{1}{2},j}(\rho_{i+2,j} - 3\rho_{i+1,j} + 3\rho_{i,j} - \rho_{i-1,j}) \tag{7}$$

Both coefficients include a normalizing factor $S_{i+\frac{1}{2},j}/\Delta t$ proportional to the length of the cell side, and $\epsilon^{(2)}_{i+\frac{1}{2},j}$ is also made proportional to the normalized second difference of the pressure

$$\nu_{i,j} = \left| \frac{p_{i+1,j} - 2p_{i,j} + p_{i-1,j}}{p_{i+1,j} + 2p_{i,j} + p_{i-1,j}} \right| \tag{8}$$

in the adjacent cells. This quantity is of second order except in regions containing a steep pressure gradient. The fourth differences provide background dissipation throughout the domain. In the neighborhood of a shockwave, ν_{ij} is order one and the second differences become the dominant dissipative terms. The dissipative terms for the other equations are constructed from similar formulas with the exception of the energy equation where the differences are of ρH rather than ρE. The purpose of this is to allow a steady-state solution for which H remains constant.

IV. Implicit Schemes

In differential form the Euler equations are

$$\frac{\partial w}{\partial t} + \frac{\partial f}{\partial x} + \frac{\partial g}{\partial y} = 0 \tag{9}$$

where f and g are flux vectors.

A prototype implicit scheme for a system of nonlinear hyperbolic equations such as the Euler equations can be formulated as

$$w^{n+1} = w^n - \beta\Delta t\left[D_x f(w^{n+1}) + D_y g(w^{n+1})\right] - (1-\beta)\Delta t\left[D_x f(w^n) + D_y g(w^n)\right] \tag{10}$$

where D_x and D_y are difference operators that approximate $\partial/\partial x$ and $\partial/\partial y$. In this form the scheme is too expensive, since it calls for the solution of coupled nonlinear equations at each time step. Let the Jacobian matrices be

$$A = \frac{\partial f}{\partial w} \qquad B = \frac{\partial g}{\partial w}$$

and let the correction be

$$\delta w = w^{n+1} - w^n$$

After linearization and dropping terms of the second and higher order, the scheme becomes

$$\left[I + \beta\Delta t(D_x A + D_y B)\right]\delta w + \Delta t R = 0 \tag{11}$$

where R is the residual

$$R = D_x f(w^n) + D_y g(w^n)$$

With $\beta = 1/2$ or 1 the scheme is second- or first-order accurate in time. Note that if $\beta = 1$ the scheme reduces to a Newton iteration in the limit $\Delta t \to \infty$. Written for an $n \times n$ mesh, Eq. (11) has a block tridiagonal form, requiring $O(n^4)$ operations for inversion. Because of this rapid growth of the operation count with n, the Newton method appears to be uncompetitive except on very coarse meshes. The scheme is reduced to an alternating direction implicit (ADI) scheme by replacing the operator of Eq. (11) by a product of two one-dimensional operators.[5,6]

$$(I + \beta\Delta t D_x A)(I + \beta\Delta t D_y B)\,\delta w + \Delta t R = 0 \tag{12}$$

Equation (12) can be inverted in two steps as

$$(I + \beta\Delta t D_x A)\,\delta w^* = -\Delta t R$$
$$(I + \beta\Delta t D_y B)\,\delta w = \delta w^* \tag{13}$$

and the operation count is now $O(n^2)$. The scheme is unconditionally stable for the linear scalar case if $\beta \geq 1/2$.

In transonic flow calculations, artificial dissipative terms must be added explicitly to capture shock waves without spurious oscillations. Since a constant coefficient dissipation formed from fourth differences cannot prevent wiggles near shock waves in fine meshes,[7] it is necessary to use adaptive dissipation of blended second and fourth differences described in Section III unless one relies on upwind or total variation diminishing schemes. Although the linear stability test shows that the scheme is unconditionally stable, explicit addition of dissipation restricts the stability bound. In order to relieve this stability bound, implicit dissipation can be inserted. After adding all dissipative terms, the scheme takes the form in one dimension

$$(I + \beta\Delta t D_x A - \epsilon^{(2)}_i \Delta t D_x^2 + \epsilon^{(4)}_i \Delta t D_x^4)\,\delta w = -\Delta t(R - \epsilon^{(2)}_e D_x^2 w + \epsilon^{(4)}_e D_x^4 w) \tag{14}$$

where D_x^2 and D_x^4 are difference operators that approximate $\partial^2/\partial x^2$ and $\partial^4/\partial x^4$ and $\epsilon^{(2)}_i$, $\epsilon^{(4)}_i$, $\epsilon^{(2)}_e$ and $\epsilon^{(4)}_e$ are coefficients of second and fourth difference dissipations. One can construct various implicit schemes by appropriate selection of the coefficients of dissipation:

1) With $\epsilon^{(2)}_i = \text{const}$ and $\epsilon^{(4)}_i = 0$, the scheme uses implicit dissipation of second differences with constant coefficient and requires block tridiagonal inversion.

2) With $\epsilon^{(2)}_i = E_1(\epsilon^{(2)}_e)$ and $\epsilon^{(4)}_i = E_2(\epsilon^{(4)}_e)$ where E_1 and E_2 are functional relationships to be determined, the scheme uses implicit dissipation of blended second and fourth differences which match explicit dissipation with variable coefficients and requires block pentadiagonal inversion.

3) With $\epsilon^{(4)}_i = \epsilon^{(4)}_e = 0$, and $\epsilon^{(2)}_i = E_1(\epsilon^{(2)}_e)$, the scheme uses second difference dissipation in both explicit and implicit parts and requires block tridiagonal inversion.

V. Multigrid Method

In order to adapt the implicit schemes for a multigrid algorithm, auxiliary meshes are introduced by doubling the mesh spacing. Values of the flow variables are transferred to a coarser grid by the rule

$$w_{2h} = \sum S_h w_h / S_{2h} \tag{15}$$

where the subscripts denote values of the mesh spacing parameter, S is the cell area, and the sum is over the four cells on the fine grid composing each cell on the coarser grid. The

rule conserves mass, momentum, and energy. The solution on a coarse grid is updated as follows:

1) Calculate the correction and update the solution on the fine grid.

2) Transfer the values of the variables to the coarse grid.

3) Collect the residual on the fine grid for the coarse grid. A forcing function is then defined as

$$P_{2h} = \sum R_h - R^t_{2h} \tag{16}$$

where R is the residual and t means the transferred value. The residual on the coarse grid is given by

$$R_{2h} = R^t_{2h} + P_{2h} = \sum R_h \tag{17}$$

4) Calculate the correction and update the solution on the coarse grid.

For the next coarser grid the residual is recalculated as

$$\begin{aligned} R_{4h} &= R^t_{4h} + P_{4h} \\ &= \sum \left(R^u_{2h} + P_{2h} \right) \\ &= \sum \left(R^u_{2h} + \sum R_h - R^t_{2h} \right) \end{aligned} \tag{18}$$

where u means the updated value. On the first coarse grid, R_{2h} is replaced by $\sum R_h$ with the result that the evolution on the coarse grid is driven by the residuals on the fine grid. The evolution on the next coarser grid is driven by an estimate of what the fine grid residuals would have been as a result of the correction on the first coarse grid.

The entire process is repeated on successively coarser grids. Finally, the correction calculated on each grid is passed back to the next finer grid by bilinear interpolation. Since the evolution on a coarse grid is driven by residuals collected from the next finer grid, the final solution on the fine grid is independent of the choice of boundary conditions on the coarse grids. The surface boundary condition is treated in the same way on every grid, by using the normal pressure gradient to extrapolate the surface pressure from the pressure in the cells adjacent to the wall. The far-field conditions can either be transferred from the fine grid, or recalculated by the procedure described in Section VII.

The interpolation of corrections back to the fine grid will introduce errors which cannot be rapidly expelled from the fine grid, and ought to be locally damped, if a fast rate of convergence is to be attained. Thus it is important that the

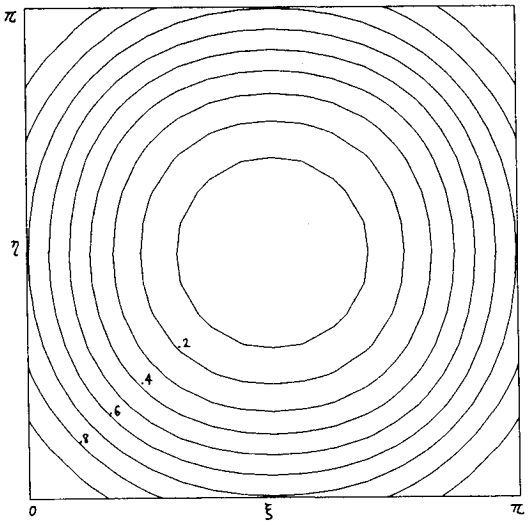

Fig. 1a Amplification factor without dissipation, $\beta = 1$.

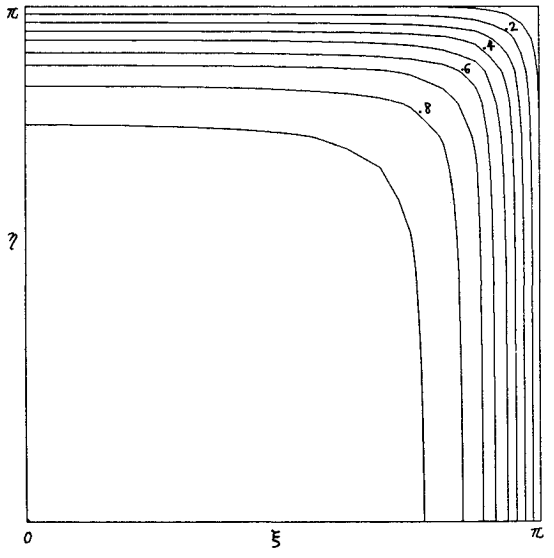

Fig. 1b Amplification factor with dissipation, $\beta = 1$.

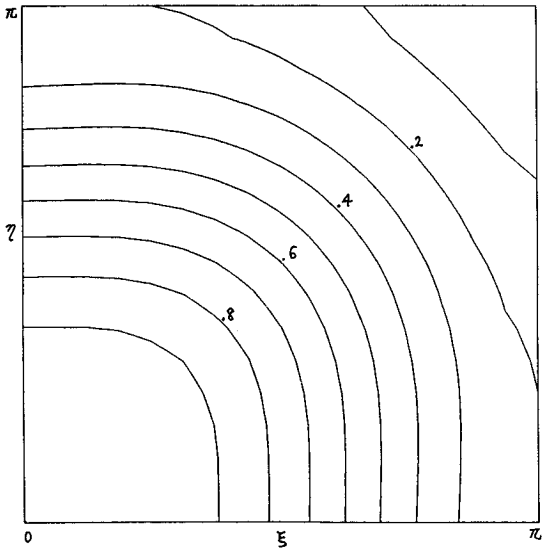

Fig. 1c Amplification factor with dissipation and optimal coefficients, $\beta = 1/2$.

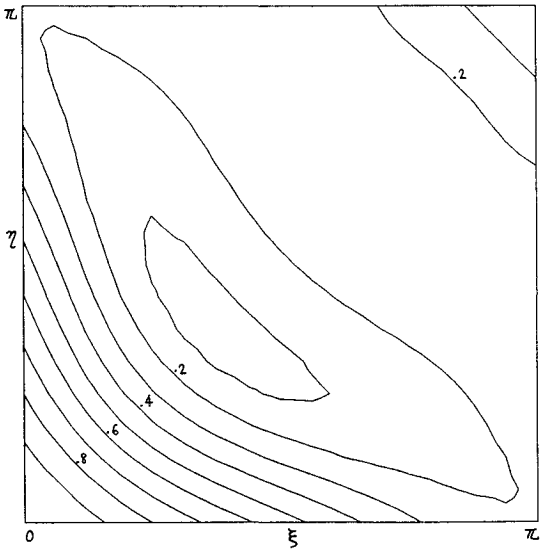

Fig. 1d Amplification factor with dissipation and optimal coefficients, $\beta = 1$.

driving scheme should have the property of rapidly damping out high frequency modes. The success of a multigrid method is critically dependent on the shape of the amplification factor. To see how the schemes can be adapted to meet this requirement we consider a model problem:

$$w_t + w_x + w_y + \epsilon_e\left(\Delta x^3 w_{xxxx} + \Delta y^3 w_{yyyy}\right) = 0 \quad (19)$$

Using the Von Neumann stability test the amplification factor $G(\xi, \eta)$ of a scheme is calculated. ξ and η denote wavenumbers. One can derive a functional relationship between the coefficients of dissipative terms which minimize the growth factor at the high frequency modes. For the above two-dimensional model problem, the relationship is given by

$$\epsilon_i = 2^{(2-m)}\lambda\left(\sqrt{2\lambda\epsilon_e} - \tfrac{1}{4}\right) \quad (20)$$

where λ is the CFL number and m is the order of implicit dissipation. With this choice of coefficients the amplification factor $G(\xi, \eta)$ should be zero at $\xi = \eta = \pi$.

Figure 1a shows the amplification factor of the scheme with $\beta = 1$ and without any dissipation. Note that the scheme is dissipative while it is not with $\beta = 1/2$. However, the scheme does not have good damping characteristic for the high frequency components. This can be improved by the addition of dissipation as shown in Fig. 1b. In this case the scheme damps out the very high frequency modes only. With the coefficients given by Eq. (20) the scheme provides heavy damping over the broad range of the high frequency modes as shown in Fig. 1c with $\beta = 1/2$ and Fig. 1d with $\beta = 1$. The scheme has better damping characteristic with $\beta = 1$ than $\beta = 1/2$. If the steady-state solution is desired, one may use $\beta = 1$ without altering the final steady state.

Several time steps might be used at each level of the multigrid cycle, but it turns out that an effective multigrid strategy is to use a simple saw tooth cycle (as illustrated in Fig. 2), in which a transfer is made from each grid to the next coarser grid after a single time step. After reaching the coarsest grid, the corrections are then successively interpolated back from each grid to the next finer grid without any intermediate Euler calculations. On each grid the time step is varied locally to yield a fixed Courant number. The same Courant number is generally used on all grids, so that progressively larger time steps are used after each transfer to a coarser grid. In comparison with a single time step on the fine grid, the total computational effort in one multigrid cycle is

$$1 + \tfrac{1}{4} + \tfrac{1}{16} + \ldots \leq \tfrac{4}{3}$$

plus the additional work of collecting residuals and interpolating the corrections. However, it has been found to be effective to use scheme 2 as explained in Section IV in the fine grid, and to use scheme 3 on the coarse grids. Since the scheme on the coarse grids needs tridiagonal inversion while the scheme on the fine grid requires pentadiagonal inversion, the additional computational effort is less than 30%. The effective time step of a complete cycle using N grid levels is approximately $(2^N - 1)\,\Delta t$ where Δt is the time step on the fine grid.

VI. Enthalpy Damping

Provided that the enthalpy has a constant value H_∞ in the far field, it is constant everywhere in a steady flow, as can be seen by comparing the equations for conservation of mass and energy. If we set $H = H_\infty$ everywhere in the flowfield throughout the evolution, then the pressure can be calculated from the equation

$$p = \frac{\gamma - 1}{\gamma}\rho\left(H_\infty - \frac{u^2 + v^2}{2}\right) \quad (21)$$

This eliminates the need to integrate the energy equation. The resulting three equation model still constitutes a hyperbolic system, which approaches the same steady state as the original system. An alternative modification is to retain the energy equation, and to add forcing terms proportional to the difference between H and H_∞.[8] Since the space discretization scheme of Section II is constructed in such a way that $H = H_\infty$ is consistent with the steady-state solution of the difference equations, these terms do not alter the final steady state. Numerical experiments have confirmed that they do assist convergence. The terms added to the mass and momentum equations are $\alpha\rho(H - H_\infty)$, $\alpha\rho u(H - H_\infty)$ and $\alpha\rho v(H - H_\infty)$, while that added to the energy equation is $\alpha\rho(H - H_\infty)$ to avoid a quadratic term in H which can be destabilizing. In multigrid calculations an effective strategy is to include these terms only on the fine grid and to increase the parameter α.

A further way of accelerating the convergence rate to a steady state is the use of a variable time step. The purpose of the variable time step is to increase the speed at which disturbances are propagated through the domain.

VII. Boundary Conditions

At a solid boundary the only contribution to the flux balance comes from the pressure. The normal pressure gradient $\partial p/\partial n$ at the wall can be estimated from the condition that $\partial/\partial t\,(\rho q_n) = 0$, where q_n is the normal velocity component. The pressure at the wall is then estimated by extrapolation from the pressure at the adjacent cell centers, using the known value of $\partial p/\partial n$.

The rate of convergence to a steady state will be impaired if outgoing waves are reflected back into the flow from the outer boundaries. The treatment of the far-field boundary condition is based on the introduction of Riemann invariants for a

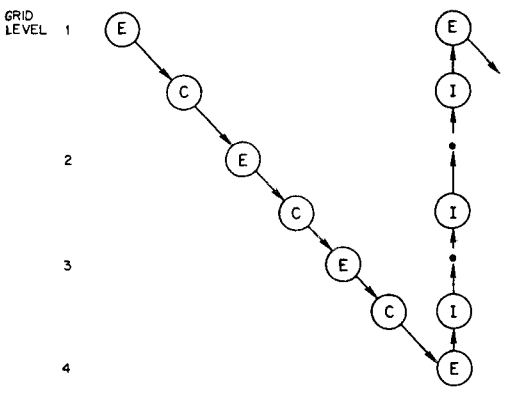

Fig. 2 Saw tooth multigrid cycle. E, Euler calculations; C, residual collection; I, interpolation.

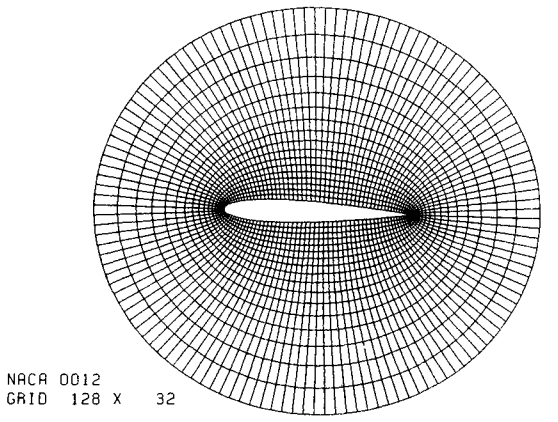

Fig. 3 O-mesh for NACA 0012.

one-dimensional flow normal to the boundary. Let subscripts ∞ and e denote free-stream values, and values extrapolated from the interior cells adjacent to the boundary, and let q_n and c be the velocity component normal to the boundary and the speed of sound. Assuming that the flow is subsonic at infinity, we introduce fixed and extrapolated Riemann invariants

$$R_\infty = q_{n\infty} - \frac{2c_\infty}{\gamma - 1}, \qquad R_e = q_{ne} + \frac{2c_e}{\gamma - 1} \tag{22}$$

corresponding to incoming and outgoing waves. These may be added and subtracted to give

$$q_n = \frac{1}{2}(R_e + R_\infty), \quad c = \frac{\gamma - 1}{4}(R_e - R_\infty) \tag{23}$$

where q_n and c are the actual normal velocity component and speed of sound to be specified in the far field. At an outflow boundary, the tangential velocity component and entropy are extrapolated from the interior, while at an inflow boundary they are specified as having free-stream values. These four quantities provide a complete definition of the flow in the far field. If the flow is supersonic in the far field, all the flow quantities are specified at an inflow boundary. In addition, they are extrapolated from the interior at an outflow boundary.

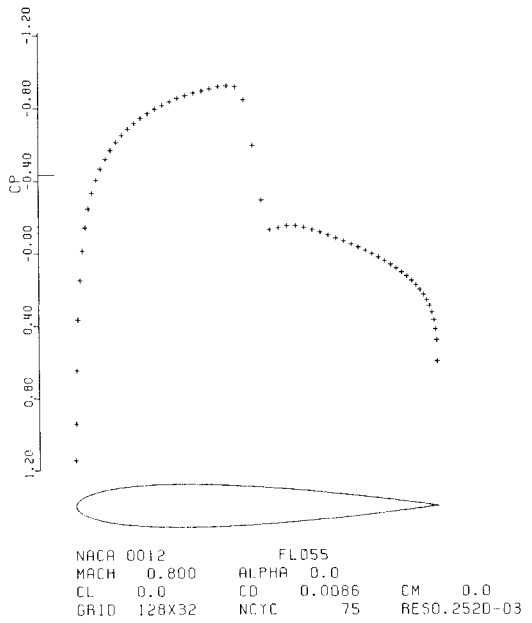

Fig. 4 Surface pressure distribution.

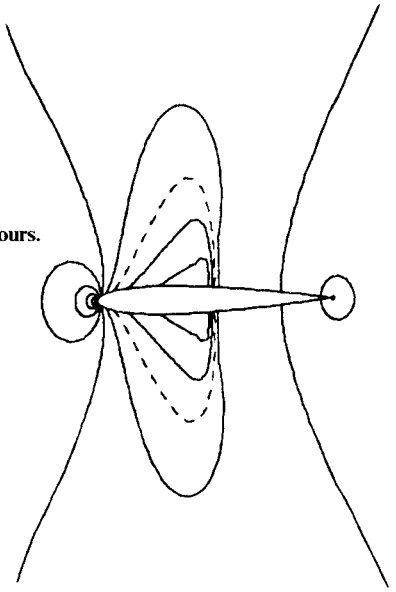

Fig. 5 Mach number contours.

VIII. Results

Two-dimensional calculations have been performed to test the multigrid method with the implicit schemes. The airfoil calculations were carried out using an O-mesh, which was generated by the method of conformal mapping, with 128

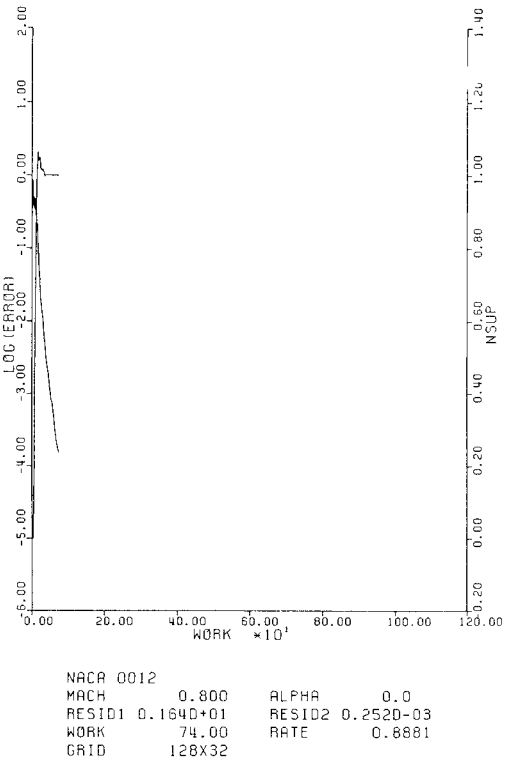

Fig. 6a Convergence history with multigrid using scheme 2.

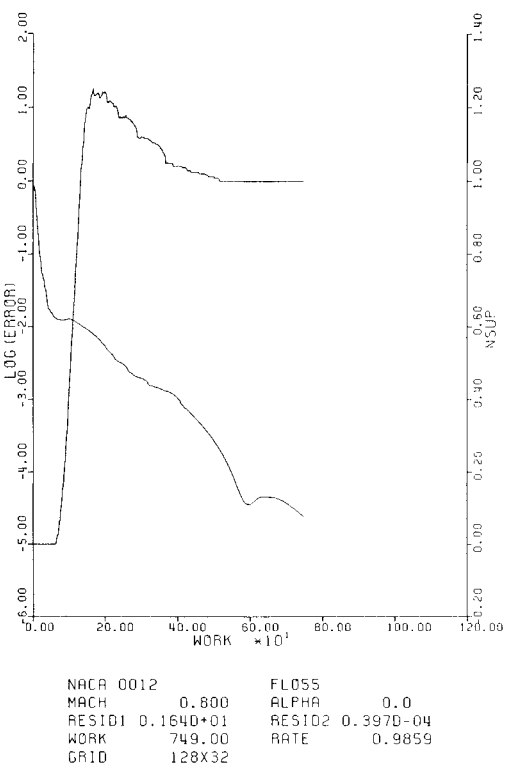

Fig. 6b Convergence history with single grid using scheme 2.

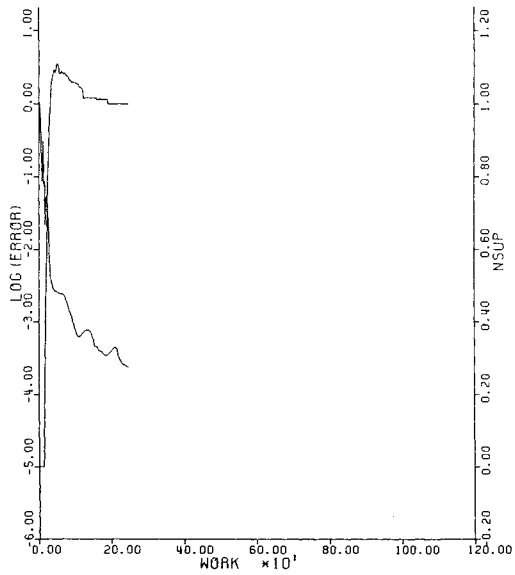

Fig. 7a Convergence history with multigrid using scheme 1.

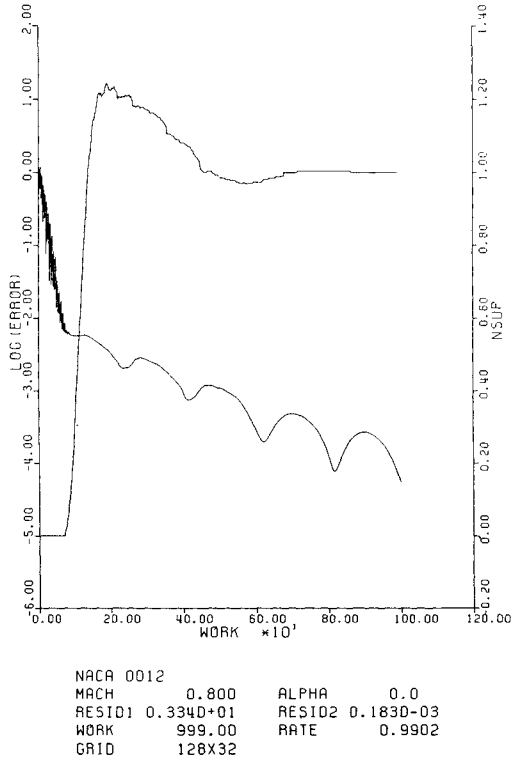

Fig. 7b Convergence history with single grid using scheme 1.

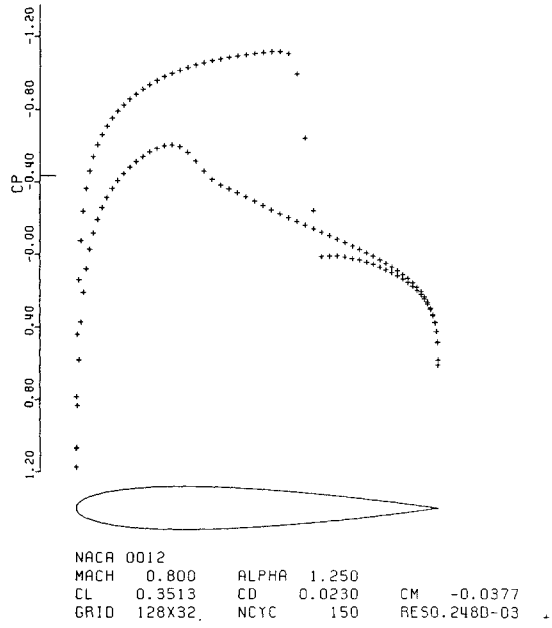

Fig. 8 Solution of a transonic lifting flow.

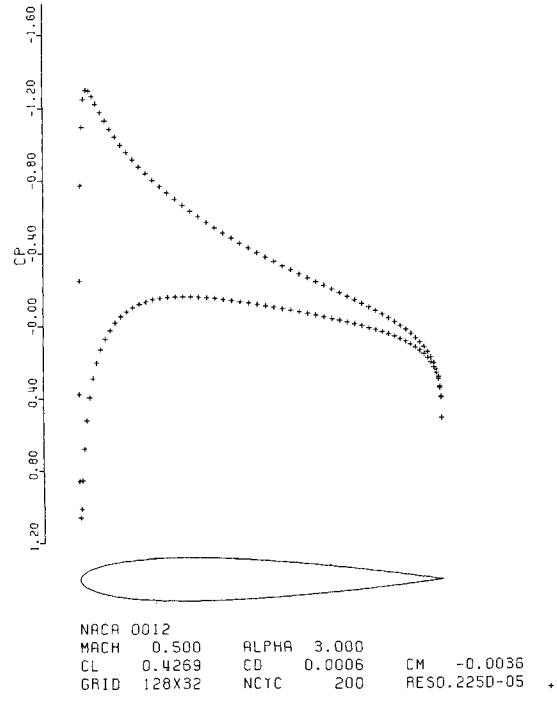

Fig. 9 Solution of a subsonic lifting flow.

intervals in the direction around the airfoil and 32 intervals in the radial direction. The mesh is shown in Fig. 3.

Figure 4 shows the pressure distribution for the NACA 0012 airfoil at Mach 0.8 and zero angle of attack, while Fig. 5 shows Mach number contours of the flowfield. The dashed line means the sonic line. Figures 6a and 6b show the convergence histories for scheme 2 in Section IV on a single grid and with multiple grids. Convergence histories for scheme 1 are shown in Figs. 7a and 7b for comparison. In each figure two indicators of the convergence rate are presented. One is the decay of the logarithm of the error where the error is measured by the root-mean-square rate of change of density on the fine grid. The other is the build-up of the number of points in the supersonic zone. For a transonic flow this indicates how quickly the supersonic zone develops and is a useful measure of the global convergence of the flowfield. With four grid levels the flowfield is fully converged in less than 50 cycles, starting from a uniform flow. Based on the buildup of the supersonic zone and the drag coefficient the multigrid method needs 40 cycles for convergence while the single grid method requires 600 cycles. The number of cycles is reduced by a factor of 15. This dramatic acceleration of convergence is achieved by the use of the scheme 2 which solves the pentadiagonal system in the fine grid and the scheme 3 which solves the tridiagonal system in the coarse grids. With scheme 1

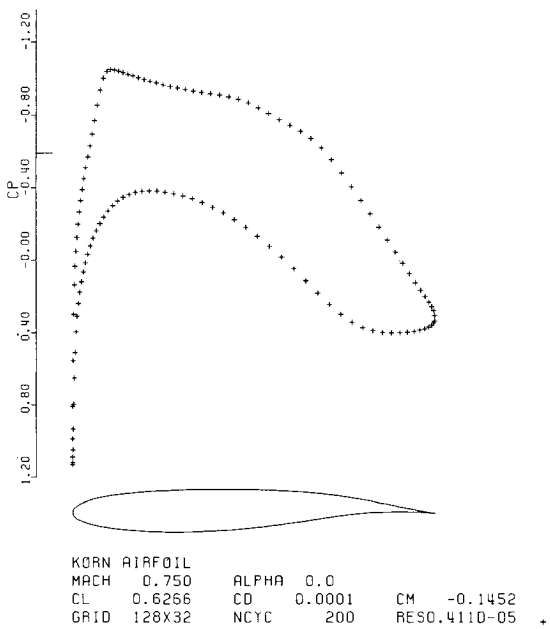

Fig. 10 Solution of a shock-free transonic flow.

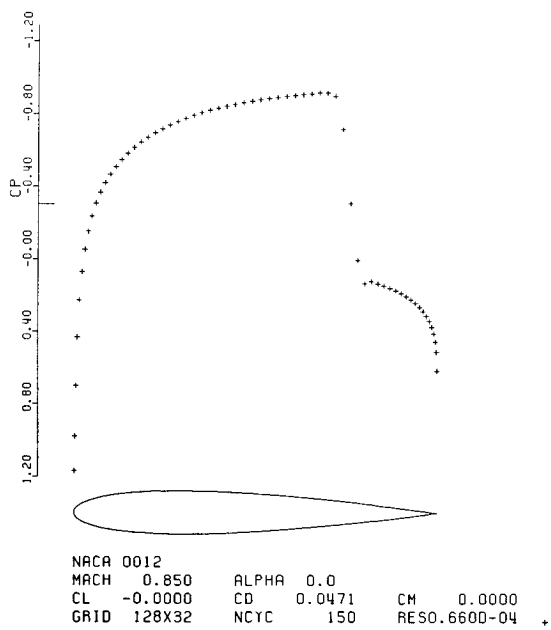

Fig. 11 Solution of a transonic nonlifting flow.

which uses the tridiagonal solver on all grids, the acceleration due to multiple grids is less impressive. The slower convergence results from the use of a constant coefficient in the implicit dissipation. These results explain the importance of high-frequency damping in multigrid through the matching of implicit and explicit dissipation.

Other examples include lifting cases. Figure 8 shows the transonic lifting case at Mach 0.8 and an angle of attack 1.25 deg. Figure 9 shows the solution of a subsonic flow over NACA 0012 airfoil at Mach 0.5 and an angle of attack of 3 deg. Figure 10 shows the case of KORN airfoil at a shock-free condition which is numerical verification of the Morawetz theorem that a shock-free transonic flow is an isolated point and that arbitrary small changes in boundary conditions will lead to the appearance of shock waves. The drag should be zero in shock-free flows like subcritical flow or KORN airfoil case; the small calculated value of drag coefficient is an indication of the level of discretization error. Finally, the solution of the transonic flow at Mach 0.85 is shown in Fig. 11.

In practice the factored schemes have a stability bound. Possible sources of this are the interactions of the factorization error at very large time steps, the nonlinearity of the problem, and the treatment of boundary conditions. However, it seems that it should be possible to take larger time steps than those used in present calculations. Even though the implicit scheme is fast, the block inversions are expensive. The computational work may be able to be decreased by using a diagonalization of the blocks which needs scalar inversions.[7]

IX. Conclusion

It is shown that a multigrid method combined with the ADI scheme can substantially accelerate the convergence of a time dependent hyperbolic system to a steady state. The solution is converged in less than 50 cycles and the achieved acceleration factor of 15 agrees well with the theoretical prediction. With the formulations here used, the steady state is entirely determined by the space discretization scheme on the fine grid. The discretization error of the present fine grid scheme is of second order in smooth regions of the flow. Further acceleration seems to be possible by achieving the potential of the implicit scheme. With the present implementation, the ADI scheme is more expensive than the multistage scheme with residual averaging. We believe that the computational work per cycle can be made comparable to that of the multistage scheme by careful coding, and it may be possible to tailor the ADI scheme to provide better performance than the multistage scheme on nonuniform grids.

References

[1]Jameson, A., "Acceleration of Transonic Potential Flow Calculations on Arbitrary Meshes by the Multiple Grid Method," AIAA Paper 79-1458, July 1979.

[2]Ni, R.H., "A Multiple Grid Scheme for Solving the Euler Equations," *AIAA Journal*, Vol. 20, Nov. 1982, pp. 1565-1571.

[3]Jameson, A., "Solution of the Euler Equations by a Multigrid Method," Princeton University, MAE Report 1613, June 1983.

[4]Jameson, A. and Baker, T.J., "Multigrid Solution of the Euler Equations for Aircraft Configurations," AIAA Paper 84-0093, Jan. 1984.

[5]Briley, W.R. and McDonald, H., "Solution of the Multidimensional Compressible Navier-Stokes Equations by a Generalized Implicit Method," *Journal of Computational Physics*, Vol. 24, No. 4, Aug. 1977, pp. 372-397.

[6]Beam, R. and Warming, R.F., "An Implicit Factored Scheme for the Compressible Navier-Stokes Equations," *AIAA Journal*, Vol. 16, April 1978, pp. 393-402.

[7]Pulliam, T.H., "Euler and Thin Layer Navier-Stokes Codes: ARC2D, ARC3D," CFD User's Workshop, University of Tennessee Space Institute, Tullahoma, TN, March 1984.

[8]Jameson, A., "Steady State Solution of the Euler Equations for Transonic Flow," *Proceedings of the Symposium on Transonic, Shock, and Multidimensional Flows*, edited by R.E. Meyer, Academic Press, New York, 1982, pp. 37-70.